International Journal of Biological Macromolecules
March 2024, Volume 260, Part 1, Pages 129483 (12p.)
https://doi.org/10.1016/j.ijbiomac.2024.129483
https://archimer.ifremer.fr/doc/00872/98399/

Multi-step semi-synthesis, structural characterization and growth factor interaction study of regiochemically sulfated diabolican polysaccharides

Esposito Fabiana [1], Sinquin Corinne [2], Colliec Jouault Sylvia [2], Cuenot Stéphane [3], Pugnière Martine [4], Ngo Giang [4], Traboni Serena [1], Zykwinska Agata [2, *], Bedini Emiliano [1, *]

[1] Department of Chemical Sciences, University of Naples Federico II, Complesso Universitario Monte S.Angelo, via Cintia 4, I-80126 Napoli, Italy
[2] Ifremer, MASAE Microbiologie Aliment Santé Environnement, F-44000 Nantes, France
[3] Nantes Université, CNRS, Institut des Matériaux Jean Rouxel, IMN, Nantes, France
[4] IRCM, Univ Montpellier, ICM, INSERM, Montpellier, France

* Corresponding authors : Agata Zykwinska, email address : Agata.Zykwinska@ifremer.fr ; Emiliano Bedini, email address : ebedini@unina.it

Abstract :

Diabolican is an exopolysaccharide (EPS) produced by Vibrio diabolicus HE800, a mesophilic bacterium firstly isolated from a deep-sea hydrothermal field. Its glycosaminoglycan (GAG)-like structure, consisting of a tetrasaccharide repeating unit composed of two aminosugars (N-acetyl-glucosamine and N-acetyl-galactosamine) and two glucuronic acid units, suggested to subject it to regioselective sulfation processes, in order to obtain some sulfated derivatives potentially acting as GAG mimics. To this aim, a multi-step semi-synthetic approach, relying upon tailored sequence of regioselective protection, sulfation and deprotection steps, was employed in this work. The chemical structure of the obtained sulfated diabolican derivatives was characterized by a multi-technique analytic approach, in order to define both degree of sulfation (DS) and sulfation pattern within the polysaccharide repeating unit, above all. Finally, binding affinity for some growth factors relevant for biomedical applications was measured for both starting diabolican and sulfated derivatives thereof. Collected data suggested that sulfation pattern could be a key structural element for the selective interaction with signaling proteins not only in the case of native GAGs, as already known, but also for GAG-like structures obtained by regioselective sulfation of naturally unsulfated polysaccharides.

Keywords : Sulfation, multi-step semi-synthesis, regioselectivity, marine polysaccharides, growth factors

1. INTRODUCTION

Sulfated glycosaminoglycans (GAGs) are complex biomacromolecules, ubiquitously distributed among vertebrates, found both in extracellular matrices and on cell surfaces. They play key roles in a plethora of physio-pathological processes, typical of higher animals (*e.g.* central nervous system development, stem cell differentiation, cancer cell progression etc.) [1]. From a structural point of view, sulfated GAGs are a family of polydisperse, linear polysaccharides that are constituted by variously sulfated, alternating aminosugars and uronic acids (or a neutral hexose, D-galactose, in a single case). Aminosugars are typically 2-acetamido-2-deoxy-D-glucopyranose (*N*-acetyl-glucosamine, GlcNAc) or 2-acetamido-2-deoxy-D-galactopyranose (*N*-acetyl-galactosamine, GalNAc), while D-glucuronic and L-iduronic acid (GlcA and IdoA, respectively) are uronic acid constituents. Depending on the monosaccharide constituents and the regio- and stereochemistry of the glycosidic bonds connecting them, sulfated GAGs can be classified into four main species: heparin/heparan

sulfate, chondroitin sulfate, dermatan sulfate and keratan sulfate. A key aspect of their structure is the distribution of sulfate groups within the repeating unit and along the polysaccharide chain. Such so called sulfation pattern can be theoretically arranged in a huge number of different combinations, nonetheless it seems to be strictly regulated *in vivo* and able to encode a variety of biological information [2].

The biological activities of sulfated GAGs made them ingredients of drugs and food supplements to treat or prevent several diseases (*e.g.* blood coagulation, articular osteoarthritis, corneal dystrophy) [3]. However, for some applications the use of natural sulfated GAGs has several limitations with respect to production costs – due to low yields and complex protocols for their isolation from animal sources –, degradability and risk of contaminations from mammalian tissues [4] in particular with harmful compounds [5]. Ethical, sustainability and regulatory concerns connected to the animal source of sulfated GAGs must be taken into consideration too. Furthermore, batch standardization is also problematic, due to the impossibility to have a precise control of sulfation pattern in GAGs from different sources. Indeed, sulfated GAGs show a significant structural heterogeneity in terms of sulfate groups distribution along the polysaccharide chain. This depends not only on animal species and tissue but also on the physio-pathological conditions of the individual animal [6,7].

The above mentioned concerns fueled in the last two decades a constantly increasing interest in accessing sulfated GAGs without employing any animal sourced material [8-10]. In this frame, chemical and chemo-enzymatic syntheses of several sulfated GAG oligosaccharides and low molecular weight polysaccharides have been reported [11-13]. Alternative approaches based on microbial cell factories [14-16] or hybrid microbiological-chemical strategies have been successfully exploited too [17, 18]. A complementary research field towards the same goal is the production of sulfated GAG mimics and analogues [19,20]. This represents a very promising topic as the obtained compounds could not only show similar structure and

bioactivities of naturally occurring sulfated GAGs, but also display improved properties that could enlarge their therapeutic applications. Indeed, the obtainment of a huge number of sulfated GAG mimics and analogues has been gained, mainly by chemical sulfation of polysaccharides from sustainable sources (plants, algae, microbes) [21,22]. The reaction is often performed under non regioselective conditions, thus allowing no access to a defined and controlled sulfation pattern in the obtained polysaccharide derivative. Therefore, detailed structure-activity relationships, relying mainly on sulfation code in naturally sulfated GAGs, cannot be inferred for artificially sulfated polysaccharides. In some cases, persulfated polysaccharide derivatives are obtained. Such products are often less interesting, because a too high level of negative charges within the polysaccharide can induce undesired, overactive responses, as clearly demonstrated in the case of per-*O* sulfated chondroitin [23]. For these reasons, the chemical research in the field has been focused on the development of regioselective methods converting polysaccharides from sustainable sources into sulfated derivatives having a well-defined distribution of sulfate groups within the repeating unit of the polymer chain. To this aim, the typical strategies are either to research direct, regioselective sulfation reactions or to tailor multi-step semi-syntheses having as key reaction the regioselective insertion of suitable protecting groups on the sites that are not intended for sulfation [24].

Among several polysaccharides subjected to such strategies, some of them are of particular interest because they show, already in their native form, a chemical structure very similar to GAGs [25-27], although without any sulfate groups decorating it. Among them, diabolican is the exopolysaccharide (EPS) produced by *Vibrio diabolicus* HE800 strain, a mesophilic bacterium firstly isolated from the polychaete annelid *Alvinella pompejana* collected from a deep-sea hydrothermal field [28]. It has showed interesting bioactive properties for skincare applications, *i.e.* promotion of fibroblast proliferation and migration and production of

extracellular matrix [29]. Diabolican has been also employed as starting material in a recent study aimed at installing sulfate groups on its GAG-like structure [30]. Measurement of the binding affinity between the obtained sulfated polysaccharide derivatives and a set of six growth factors, revealed a much stronger binding for the per-*O*-sulfated derivatives with respect to the polysaccharides having a low sulfate content. Furthermore, a per-*O*-sulfated derivative was very recently shown to be efficient in preventing brain inflammation and metabolism failure in mucopolysaccharidosis IIIA mice [31]. However, less sulfated diabolican derivatives with specific sulfation patterns may offer the possibility to finely tune the binding affinity towards signaling proteins with more selective interactions when compared to oversulfated derivatives. To this aim, the semi-synthesis of a new set of diabolican derivatives with intermediate DS values leading to specific sulfation patterns has been undertaken in this work. Their affinity for some growth factors, relevant for biomedical applications, has been investigated too.

2. EXPERIMENTAL SECTION

2.1. General methods. Commercial grade reagents and solvents (HPLC-grade pure, including water) were used without further purification, except where differently indicated. Dialyses were conducted on Spectra/Por 3.5 kDa cut-off membranes at 4°C. Centrifugations were performed with an Eppendorf (Hamburg, Germany) Centrifuge 5804R instrument at 4°C (4600 g, 5 min). Freeze-dryings were performed with a 5Pascal (Trezzano sul Naviglio, Italy) Lio 5P 4K freeze dryer. Elemental analyses were performed on a ThermoFisher Scientific (Waltham, MA, USA) Flash Smart V CHNS/CHNS instrument, using sulfanilamide as calibration standard.

The weight-average (M_w) and number-average (M_n) molecular weights were determined using high-performance size-exclusion chromatography (HP-SEC) coupled with a multi-angle laser

light scattering detector (MALLS, Dawn Heleos-II, Wyatt Technology, Santa Barbara, CA, USA) and a differential refractive index (RI) detector (Optilab Wyatt technology, Santa Barbara, CA, USA). HP-SEC system was composed of an HPLC system Prominence (Shimadzu, Kyoto, Japan), a PL aquagel-OH MIXED, 8 µm guard column (7.5 × 50 mm, Agilent Technologies, Santa Clara, CA, USA), and a PL aquagel-OH MIXED separation column (7.5 × 300 mm, Agilent Technologies, Santa Clara, CA, USA). Samples (in duplicate) were eluted with aqueous 0.1 M NH_4OAc at 1 mL/min flow rate. Molecular weights were calculated using a refractive index increment characteristic of polysaccharides, dn/dc = 0.145 mL/g.

IR spectra of diabolican derivatives were recorded using VERTEX 70 FTIR spectrometer (Bruker, Billerica, MA, USA) in ATR mode in the range 4000−500 cm^{-1}. NMR spectra were recorded on a Bruker (Billerica, MA, USA) Avance-III HD (^1H: 400 MHz, ^{13}C: 100 MHz) or on a Bruker Avance-III (^1H: 600 MHz, ^{13}C: 150 MHz) instrument – the latter equipped with a cryo-probe – in D_2O (acetone as internal standard, ^1H: $(CH_3)_2CO$ at δ 2.22 ppm; ^{13}C:$(CH_3)_2CO$ at δ 31.5 ppm) or DMSO-d_6 (^1H: CHD_2SOCD_3 at δ 2.49 ppm; ^{13}C: CD_3SOCD_3 at δ 39.5 ppm). Data were processed using the data analysis packages integrated with Bruker TopSpin® 4.0.5 software. Gradient-selected COSY, TOCSY and NOESY experiments were performed using spectral widths of 6000 Hz in both dimensions, using data sets of 2048 × 256 points. TOCSY mixing time was set to 120 ms. ^1H,^{13}C-DEPT-HSQC and ^1H,^{13}C-HSQC-TOCSY experiments were measured in the ^1H-detected mode via single quantum coherence with proton decoupling in the ^{13}C domain, using data sets of 2048 × 256 points and typically 100 increments. The mixing time for ^1H,^{13}C-HSQC-TOCSY was set to 120 ms.

Transforming Growth Factor-β1 (TGF-β1), Bone Morphogenetic Protein-2 (BMP-2), Vascular Endothelial Growth Factor ($VEGF_{165}$) and Fibroblast Growth Factor-2 ($FGF\text{-}2_{146}$) from PeproTech (ThermoFisher Scientific, Waltham, MA, USA) were covalently immobilized

(3400-4800 RU) to the dextran matrix of a CM5 sensor chip (Cytiva, Washington, DC, USA) by amine coupling, as recommended by the manufacturer at a flow rate of 5 µL/min. Binding assays of diabolican derivatives were performed in 10 mM HEPES at pH 7.4 containing 150 mM NaCl and 0.005% P20 surfactant (HBS-P buffer, Cytiva, Washington, DC, USA) by one-cycle kinetic titration. Five increasing concentrations (12 – 37 – 111 - 333 – 1000 nM) were injected (injection time =180s) at 30 µL/min. After a dissociation time of 600 s coated surface was regenerated using 4.5 mM NaOH. All the sensorgrams were corrected by subtracting the low signal from the control reference surface and buffer blank injections. From the resulting sensorgrams, KD were evaluated using a bivalent fitting model from T200 evaluation software (Cytiva, Washington, DC, USA).

2.2. Native and LMW diabolican. Native diabolican was produced by the deep-sea hydrothermal vent bacterium *V. diabolicus* in a bioreactor, according to previously published studies [28,31]. LMW diabolican was prepared using free-radical depolymerization process followed by purification through gel filtration chromatography, as already described [29].

*2.3. Derivative **2***. Derivative **1** [30] (27.3 mg) was suspended in dry methanol (3.5 mL) and then treated with a 2.0 M solution (0.7 mL) of (trimethylsilyl)diazomethane ($TMSCHN_2$) in diethyl ether (Et_2O). After 2 hours stirring at room temperature, a second aliquot (0.7 mL) of the $TMSCHN_2$ solution was added. After further 2 hours stirring, the yellow reaction mixture was treated with diisopropyl ether (20 mL) to afford a white precipitate that was collected by centrifugation and dried under vacuum to give derivative **2** (11.6 mg, 42% weight yield).

*2.4. Derivatives **3-5***. Derivative **1** [30] (20.8 mg) (or **2** for the semi-synthesis of **5**) was suspended in dry *N*,*N*-dimethylformamide (DMF, 0.8 mL) and then treated with *t*-butyl-dimethylsilyl chloride (TBDMSCl, 12.5 mg) or triisopropylsilyl chloride (TIPSCl, 15.8 mg) and imidazole (16.3 mg). The reaction mixture was stirred overnight at 50°C. Thereafter, it was cooled to room temperature and treated with diisopropyl ether (3.5 mL). The obtained

precipitate was collected by centrifugation and dried under vacuum to give derivative **3** (16.1 mg, 77% weight yield) or **4** (30.8 mg, 148% weight yield) or **5** (14.5 mg, 70% weight yield).

*2.5. Derivatives **6-8***. LMW diabolican [30] (20.5 mg) was dissolved in water (1.0 mL) and passed through a short Dowex 50 WX8 column (H^+ form, 20–50 mesh, approx. 4 cm^3). Elution with water was continued until a neutral pH of the eluate was detected. The eluted fraction was freeze-dried to give a white solid (20.5 mg), that was stirred at 80 °C for 1 hour in dry DMF (1.0 mL) to give a homogeneous solution. This was then treated at room temperature with anisaldehyde dimethyl acetal (*p*-OMe-PhCH(OCH_3)$_2$, 45 μL), that was dried over freshly activated AW-300 4Å molecular sieves. A freshly prepared 0.87 M solution of CSA in dry DMF (7.3 μL) was then added and the reaction mixture was heated at 80 °C. After overnight stirring, it was cooled to room temperature and, for the semi-synthesis of **6**, treated with diisopropyl ether (5 mL) to give a yellowish precipitate. The mixture was stored at −28 °C for some hours, then the solid was collected by centrifugation and dried under vacuum to afford derivative **6** (26.6 mg, 130% weight yield).

Conversely, for the semi-synthesis of **8**, after overnight stirring at 80°C and cooling to rt, the reaction mixture was one-pot treated with a 2:1 v/v CH_3CN-DMF mixture (750 μL) and then triethylamine (Et_3N, 74 μL), acetic anhydride (Ac_2O, 100 μL) and 4-dimethylaminopyridine (DMAP, 1.2 mg) were consecutively added. After overnight stirring at 50°C, the reaction mixture was cooled to room temperature and then treated with diisopropyl ether (10 mL) to afford a brownish precipitate. The mixture was stored at −28 °C for some hours, then the solid was collected by centrifugation and dried under vacuum to afford derivative **7** (25.5 mg), that was dissolved in a 9:1 v/v mixture (1.0 mL) of acetic acid (AcOH) and water and stirred at 50°C for 48 hours. The reaction mixture was then cooled to room temperature, diluted with water (3.0 mL), dialyzed and freeze-dried to afford derivative **8** (18.7 mg, 91% weight yield from LMW diabolican).

*2.6. Derivative **10***. Compound **1** [30] (25.2 mg) was stirred under an argon atmosphere at 85 °C for 1 hour in dry DMF (1.0 mL) to give a homogeneous solution, that was then cooled to room temperature, treated with benzoic anhydride (Bz_2O, 138 mg) and then heated to 85°C. After 24 hours stirring, the solution was cooled to room temperature and treated with dry pyridine (870 μL) and DMAP (5.0 mg). The yellowish solution was stirred for 68 hours and then treated with methanol (870 μL) and sodium acetate (NaOAc, 2.5 mg). After 26 h stirring at room temperature, the reaction mixture was diluted with methanol (2.4 mL) and then concentrated by rotoevaporation to approximately 2 mL in volume. Cold diisopropyl ether (5 mL) was added to the residue, to give a slightly yellow precipitate. The mixture was stored at −28 °C for some hours, then the solid was collected by centrifugation and dried under vacuum to afford derivative **10** (32.0 mg, 127% weight yield).

*2.7. Derivatives **SD-5-7***. Compound **6** (24.1 mg) (or **8** or **10** for the semi-synthesis of **SD-6** or **SD-7**, respectively) was stirred for few minutes at 50 °C in dry DMF (675 mL) to give a yellowish, homogeneous solution, that was then cooled to room temperature and treated with a 0.42 M solution of pyridine–sulfur trioxide complex (SO_3·py) in dry DMF (1.3 mL). After overnight stirring at 50 °C, a cold saturated NaCl solution in acetone (7 mL) was added at room temperature and the mixture was then stored at -28 °C for some hours to give a precipitate, that was collected by centrifugation and then dissolved in pure water (2.0 mL). For the semi-synthesis of **SD-5**, the resulting acid mixture (pH ~ 2) was heated to 50 °C and stirred for 2 hours. Thereafter, the mixture was cooled to room temperature and neutralized with a 33% w/v NaOH aqueous solution. After dialysis and freeze-drying, sulfated polysaccharide **SD-5** (24.6 mg, 102% weight yield) was obtained as a slightly yellow solid, that was further purified for biological assays by consecutive filtration on two C-18 silica gel cartridges.

For the semi-synthesis of **SD-6,7**, the acid mixture resulting after suspending the sulfated precipitate in water, was directly treated with a 33% w/v NaOH aqueous solution to alkaline

pH (≥ 12). After overnight stirring at room temperature, the resulting homogeneous solution was neutralized with 1M HCl, dialyzed and freezed-dried to afford **SD-6,7**. Their further purification was performed as described above for derivative **SD-5**.

2.8. Degree of sulfation. For the evaluation of the DS by CHNS elemental analysis, **SD-5-7** samples (~2-3 mg) were weighted and mixed in a tin capsule with V_2O_5 as oxidizer. They were then combusted in a furnace with the following set of parameters: temperature furnace = 950 °C, temperature oven = 65 °C, He carrier flow = 140 mL/min, O_2 flow = 250 mL/min flow, oxygen injection end = 3 s, sampling delay time = 12 s, run time = 720 s. Experiments were performed for each sample in duplicate. DS values were calculated according to Eq. (1) (m_C = atomic mass carbon, m_S = atomic mass sulfur, n_C = number of carbon atoms per repeating unit).

$$DS = [(\%S \times m_C \times n_C)/(\%C \times m_S)] \quad \text{Eq. (1)}$$

3. RESULTS AND DISCUSSION

3.1. Semi-synthesis.

Native diabolican has a high molecular weight polysaccharide chain (> 1 MDa) showing a tetrasaccharide repeating unit composed of β-1→4-GlcNAc, two consecutive β-1→4-linked GlcA and α-1→3-GalNAc residues (Fig. 1) [32, 33]. After its partial, free-radical depolymerization to give a low molecular weight (LMW) polysaccharide (M_w = 24.0 ± 0.1 kDa), the application of either an exhaustive sulfation reaction [34] or some regioselective approaches afforded a set of four sulfated diabolican derivatives (**SD-1-4**, Fig. 1), with different molecular weight distributions and/or degrees of substitutions (DSs) [30]. In particular, the latter parameter – defined as the average number of sulfate groups per polysaccharide repeating unit – was equal to 8 in the case of per-*O*-sulfated derivatives **SD-3** and **SD-4**, *i.e.* all the eight available sites per tetrasaccharide repeating unit were decorated with sulfate groups. Conversely, derivatives **SD-1** and **SD-2** showed a low DS value (1 and 1.5, respectively).

The obtainment of diabolican derivatives with intermediate DS values was tackled in this work by testing properly tailored, multi-step semi-synthetic sequences. These relied upon the regioselective introduction of protecting groups at some of the eight hydroxyls of diabolican repeating unit, followed by sulfation of the still unprotected alcohol moieties and then by deprotection of the sulfated polysaccharide derivative. The protection of diabolican with sterically hindered protecting groups was firstly tried, in order to protect the most accessible positions of the polysaccharide. To this aim, two silyl ether protecting groups (*t*-butyldimethylsilyl, TBDMS and triisopropylsilyl, TIPS) were selected on the basis of their successful employment on polysaccharides such as cellulose [35] and alginate [36]. Therefore, after a cation exchange step converting LMW diabolican into its *n*-tetrabutylammonium (TBA) salt **1** [30], the latter was treated with TBDMSCl or TIPSCl in the presence of imidazole in DMF (Scheme 1). After purification by precipitation, obtained derivatives **3** and **4** were subjected to ^{1}H-NMR analysis. This showed the absence of any silyl ether moiety covalently linked to the polysaccharide, as no significant signal was detected in the typical regions for $SiCH_3$ (at approx. 0.0-0.1 ppm) and $SiCH(CH_3)_2$ (at approx. 1.0-1.1 ppm) moieties of TBDMS and TIPS groups, respectively (Fig. S2-S3 in Supporting Information). The same result was observed by performing the TBDMS installation on diabolican methyl ester derivative **2** (Fig. S4 in Supporting Information), that could be obtained in turn by treating **1** with trimethylsilyl diazomethane ($TMSCHN_2$) in a methanol-ether mixture (Scheme 1).

A second approach to the regioselective protection of LMW diabolican relied upon the employment of cyclic protecting groups (Scheme 2), in order to protect two reactive moieties of the polysaccharide repeating unit in a single step. In particular, a *p*-methoxy-benzylidene acetal group was selected among the several cycling protecting groups already developed in synthetic carbohydrate chemistry [37]. *p*-Methoxy-benzylidene rings are known to protect preferentially 1,2-*cis*-configured diols and 1,3-diols composed of at least one primary hydroxyl

group. Diabolican repeating unit contains only a single example of the latter kind of diols, *i.e.* at positions 4 and 6 of GlcNAc residue. Therefore, the *p*-methoxy-benzylidenation reaction on LMW diabolican conducted with *p*-OMe-PhCH(OCH_3)$_2$ and CSA in DMF at 80°C was expected to afford the regioselective protection of GlcNAc hydroxyls without any reaction on the other six alcohol moieties of diabolican repeating unit. The presence of *p*-methoxy-benzylidene rings on **6** was confirmed by its ^{1}H-NMR spectrum, that showed some signals in the region between 6.80 and 7.60 ppm, clearly ascribable to the aromatic ring of the cyclic protecting group (Fig. 2). The successful *p*-methoxy-benzylidenation reaction was included also in a three steps, two pot sequence [38]. This consisted in the cyclic protecting group installation, followed by acetylation of the secondary hydroxyl groups on GlcA and GalNAc residues and then by chemoselective cleavage of the *p*-methoxybenzylidene rings to restore the diol moiety on GlcNAc units. This sequence was expected to afford derivative **8** with a free hydroxyl groups pattern complementary to derivative **6**. The presence of acetyl ester groups in the structure of **8** was confirmed by the signals at 1.96-2.15 ppm in its ^{1}H-NMR spectrum. Instead, no signals were detected in the aromatic region, thus confirming the successful cleavage of the *p*-methoxybenzylidene protecting groups (Fig. 2).

A third approach to protect some defined positions of LMW diabolican repeating unit was based on an intramolecular reaction, involving the carboxylic acid and the alcohol group at position 3 of GlcA residues, to form a lactone ring. This reaction has been recently transferred with success from monosaccharides to polysaccharides field [39], by employing Bz_2O in DMF at 85°C. Therefore, it was conducted on LMW diabolican under such reaction conditions, followed by one-pot treatments firstly with DMAP and pyridine at room temperature to allow the benzoylation of all the free hydroxyls and then with sodium acetate and methanol to cleave the lactone rings on GlcA units. This three step, one pot procedure was expected to afford derivative **10**, having all the reactive moieties of diabolican repeating unit protected as esters

but the hydroxyls at position 3 of the two GlcA residues (Scheme 2). The presence of Bz esters in the structure of **9** was confirmed by its ^{1}H-NMR spectrum, displaying a group of intense, broad signals in the region between 7.2 and 8.1 ppm, typical for Bz esters phenyl rings (Fig. 2).

Partially protected diabolican derivatives **6**, **8** and **10** were subjected to sulfation under standard conditions with SO_3· py in DMF at 50 ° C, followed by a treatment under acid or alkaline aqueous conditions, in order to remove the *p*-methoxy-benzylidene protecting groups of **6** or the ester moieties of **8** and **10**, respectively, and afford the target derivatives **SD-5-7** (Fig. 3).

3.2. Structural characterization. After purification by dialysis, products **SD-5-7** were subjected to a multi-technique structural analysis. First, their weight-averaged molecular weight (M_w) and dispersity were evaluated by HP-SEC-MALLS analysis. M_w values were found to be slightly to significantly shortened with respect to starting LMW diabolican, although a dramatic fragmentation of the polysaccharide chain was not noted in all cases (Table 1). Similarly, a slight to significant increase of dispersity was detected. With respect to the decoration of **SD-5-7** structures with sulfate groups, this was ascertained by CHNS elemental analysis and ATR-FT-IR spectroscopy. The former investigation confirmed, for all the three derivatives, not only the presence of sulfur atoms in their structures but also intermediate DS values spanning from 1.27 to 3.85, as pursued. Infra-red spectroscopy analysis confirmed that sulfur atoms were embedded in sulfate groups. This was clearly indicated by the appearance of signals at 1218-1226 and 804-806 cm^{-1} in the ATR-FT-IR spectra of **SD-5-7**, not present in LMW diabolican one and accounting for asymmetric O=S=O and symmetric C-O-S stretching vibrations, respectively (Fig. S22 in Supporting Information).

In order to gain insights on sulfate group distribution on **SD-5-7** backbones, ^{1}H- and 2D-NMR spectra were measured for these derivatives. Both their ^{1}H and ^{1}H,^{13}C-DEPT-HSQC

spectra (Fig. S9, S12 and S17 in Supporting Information) did not show any signal ascribable to non-polysaccharide, contaminant species. This attested a satisfying purity grade for all the three derivatives. As for the $^{1}H,^{13}C$-DEPT-HSQC spectrum of **AS-5 (**Fig. 4A), its comparison with LMW diabolican one (Fig. S10 in Supporting Information) clearly revealed the ^{1}H- and ^{13}C-downfield shift of a single methylene signal associated to primary positions of aminosugars, in particular the one related to CH_2 atoms at position 6 of GalNAc residues. This suggested, as expected, that this position was quantitatively sulfated in **SD-5**, while GlcNAc primary hydroxyls were not sulfated at all. As for the anomeric signals, the most ^{1}H-downfield shifted one at $\delta_{H/C}$ 5.56/96.2 was easily assigned to GalNAc units due to their exclusive α-configuration among anomeric sites of diabolican repeating unit (Table 2). This signal displayed a clear COSY correlation (Fig. 4B) with the two most ^{13}C-upfield shifted CH signal at $\delta_{H/C}$ 4.57/47.8 and 4.45/47.8, that could both assigned to CH groups on the nitrogen atom of GalNAc residues, evidently affected by two slightly different chemical environments. By the analysis of HSQC-TOCSY signals correlating with GalNAc anomeric signal, a single signal related to CH atoms at position 3 of GalNAc units could be found at $\delta_{H/C}$ 4.44/74.7 (Fig. 4A). Its marked ^{1}H- and ^{13}C- downfield shift with respect to the signal at $\delta_{H/C}$ 3.89/69.2 [30] associated to the same CH atoms in LMW diabolican, revealed that GalNAc O-3 atom was quantitatively decorated with a sulfate group in **SD-5**, in agreement with the semi-synthetic strategy to obtain it. The homogeneity of the 3,6-disulfation pattern on GalNAc units suggested that the different chemical environment splitting their CH-2 atoms in two magnetically different populations was due to a structural heterogeneity on vicinal units, *i.e.* GlcNAc or GlcA residues. The former showed all the signals neither ^{1}H- nor ^{13}C-downfield shifted with respect to the starting polysaccharide, therefore confirming the expected absence on any sulfate group installed on GlcNAc units. Conversely, the signal of anomeric CH atoms of the two GlcA residues were split in three different peaks. The most intense one ($GlcA_I$ CH-1) resonated at $\delta_{H/C}$ 4.93/100.0

and the other two ($GlcA_{II}$ and $GlcA_{III}$ CH-1) at $\delta_{H/C}$ 5.07/100.2 and 4.80/102.2, respectively (Table 2 and Fig. 4A). The three peaks were all ^{1}H-downfield and ^{13}C-upfield shifted with respect to GlcA anomeric signals in unsulfated LMW diabolican (at $\delta_{H/C}$ 4.68/104.7 and 4.53/104.2) [30]. This behavior [40] suggested that $GlcA_{I-III}$ units were all derivatized with sulfate groups at positions 2 and/or 3. Since the anomeric signals for $GlcA_{II}$ and $GlcA_{III}$ showed a similar intensity, that was lower with respect to the $GlcA_{I}$ one, a heterogeneous sulfation pattern for one of the two GlcA residues of **SD-5** could be hypothesized. This was confirmed by detecting the $GlcA_{I-III}$ H-1-H-2 cross-peaks in COSY spectrum and the HSQC-TOCSY signals correlating with $GlcA_{I-III}$ anomeric signals. Indeed, it was possible to locate the CH-2 signal of $GlcA_{I}$ and $GlcA_{II}$ at much higher ^{1}H and ^{13}C chemical shift values ($\delta_{H/C}$ 4.33/77.2) with respect to $GlcA_{III}$ one ($\delta_{H/C}$ 3.60/72.2). Since the ^{1}H chemical shift value assigned to the former was close to the one reported for LMW per-*O*-sulfated diabolican (δ_{H} 4.42-4.46 [30]; see also Fig. S11 in Supporting Information), $GlcA_{I}$ and $GlcA_{II}$ were both assigned as 2,3-disulfated residues. Conversely, $GlcA_{III}$ could be recognized as a 3-sulfated unit because its CH-3 atoms – but not CH at position 2 – showed a marked ^{1}H- and ^{13}C-downfield shifted signal at $\delta_{H/C}$ 4.49/81.6 (as detected by H-1-H-3 cross-peak in TOCSY spectrum and by CH-1-CH-3 correlation in HSQC-TOCSY spectrum) with respect to unsulfated LMW diabolican ($\delta_{H/C}$ 3.60/78.3). This suggested an unexpected, heterogeneous sulfation pattern for either GlcNAc- or GalNAc-linked GlcA residue. The GlcNAc-H-1-$GlcA_{I}$-H-4 cross-peak at $\delta_{H/H}$ 4.66/4.39 in NOESY spectrum together with the HSQC-TOCSY signal at $\delta_{H/H}$ 4.39/100.0 allowed to discriminate between these two possibilities. In particular, they revealed that GlcNAc-linked GlcA residues were 2,3-di-*O*-sulfated, while GalNAc-linked GlcA units were all sulfated at their 3-*O*-position and only to a limited extent at *O*-2 site. The relative integration in the $^{1}H,^{13}C$-DEPT-HSQC spectrum of the anomeric signal volumes for $GlcA_{II}$ and $GlcA_{III}$ allowed estimating a 31:69 ratio for GalNAc-linked GlcA2,3S and GlcA3S units in **SD-5**, assuming that

the signals displayed similar $^{1}J_{C,H}$ coupling constants and that a difference of around 5−8 Hz from the experimental set value did not cause in any case a substantial variation of the integrated peak volumes [41,42]. To summarize, by 2D-NMR analysis **SD-5** was detected to have a sulfation pattern in good agreement with the expected one (Table 1 and Fig. 3), *i.e.* with sulfate groups placed on both GalNAc and the two GlcA residues of diabolican repeating unit, and no sulfation on GlcNAc residues.

The distribution of sulfate groups decorating diabolican backbone was investigated by 2D-NMR spectroscopy also for derivatives **SD-6,7**. ^{1}H and ^{13}C chemical shift assignments are reported in Table 2. DS values were estimated for any single sulfated positions again by ^{1}H,^{13}C-DEPT-HSQC peak volumes integration. For **SD-6** a sulfation pattern complementary to **SD-5** one was expected, *i.e.* with sulfate groups decorating positions 4 and 6 of GlcNAc units exclusively. Indeed, the presence of sulfate groups on these sites was confirmed by 2D-NMR analysis. Nonetheless, a quantitative derivatization was found only for the primary position, while only a 48% average amount of sulfate groups was estimated for the GlcNAc *O*-4 site along the polysaccharide backbone. Furthermore, an unexpected 51% average amount of sulfate groups was found on GlcA *O*-2 positions, together with a minor amount (19%) estimated for GlcA *O*-3 sites. Noteworthy, a partial sulfation of GlcA *O*-2 positions was in agreement with the non-quantitative sulfation at the same sites in derivative **SD-5**. These complementary results could be hypothetically ascribed to the formation of acyclic acetals protecting some GlcA units during the *p*-methoxy-benzylidenation reaction of LMW diabolican to **6** and **7**, as already reported for the acetalation of some polysaccharides (*e.g.* dextran [43] and *E. coli* sourced chondroitin-like exopolysaccharide [44]). Nonetheless, further experimentation is necessary to shed light on this point. It is beyond the scope of this work and will be reported elsewhere.

With respect to derivative **SD-7**, the employed strategy through intermediates **9** and **10** (Scheme 2) suggested the presence of sulfate groups placed at positions *O*-3 of GlcA units.

Instead, they could not be detected by 2D-NMR analysis. Conversely, sulfation was found to occur at position 3 of some GalNAc residues and at position 4 of some GlcNAc units (Table 2, Fig. 3 and S19 in Supporting Information). This unexpected sulfation pattern could be ascribed to the absence of any 3,6-lactone rings in compound **9** (Scheme 2). Therefore, the following benzoylation reaction was allowed to protect all the hydroxyls of diabolican backbone, leaving the alcohol functionality still free only on some of the most plausibly hindered positions, *i.e.* GalNAc *O*-3 and GlcNAc *O*-4 sites. Such unprotected positions were in turn derivatized with sulfate groups in the subsequent reaction from derivative **10** to product **SD-7**.

3.3. Binding affinity of diabolican derivatives with growth factors.

Biological activities of sulfated GAGs result from their protein-binding ability, allowing regulation of both physiological and pathological processes [45,46]. GAG-protein interactions depend on several factors, including molecular weight, degree and pattern of sulfate groups present on the polysaccharide backbone. It was recently shown that per-*O*-sulfated diabolican derivatives (DS 8) strongly bind positively charged growth factors, *e.g.* TGF-β1, BMP-2, VEGF, GDF-5 and FGF-2 [30]. For the same sulfation pattern, the binding affinity was higher for the derivative with lower molecular weight. In contrast, interactions between less sulfated derivatives having a DS ranging from 0 to 1.5 and growth factors were considerably decreased [30]. Herein, the binding affinity between diabolican derivative **SD-5** and TGF-β1 and BMP-2 was only slightly diminished with respect to per-*O*-sulfated derivative **SD-4** (Table 3). Conversely, a much stronger binding was measured for FGF-2, not only with respect to **SD-4** but also to heparin [30,47]. Binding between FGF-2 and heparin was shown to be based on electrostatic interactions, hydrogen bonding and van der Waals forces, involving basic and polar amino acid residues (K135, Q134, N27, R120, K119, K129). In particular, Q134 and N27 interacted with the critical sulfate groups placed at *O*-2 and *N*-2 atoms of L-iduronic acid (IdoA)

and GlcNAc residues of heparin, respectively [48]. Furthermore, although the *O*-6 sulfate group in GlcNAc was not directly involved in FGF-2 binding, in contrast to FGF-1 [49,50], its presence was required to induce the interaction of FGF-2 with its FGFR receptor [51]. Analogously, sulfate groups at GlcA-*O*-2 and GalNAc *O*-6 positions in diabolican derivative **SD-5** could be responsible for its high FGF-2 binding affinity. Other sulfated positions on GalNAc-*O*-3 and GlcA-*O*-3 may additionally contribute to the overall interaction with FGF-2. Interestingly, for less sulfated derivatives **SD-6** and **SD-7**, similar binding affinities in comparison to **SD-5** were measured toward TGF-β1, BMP-2 and VEGF, while their interaction with FGF-2 was considerably decreased (in the case of **SD-6** even to a weaker affinity with respect to unsulfated LMW diabolican). Altogether, new diabolican derivatives of intermediate DS with specific sulfation patterns and displaying high binding affinities with some of investigated growth factors, seem promising as GAG mimetic candidates for some biomedical applications, especially in regenerative medicine field.

4. CONCLUSIONS

Three derivatives of the GAG-like diabolican polysaccharide, carrying sulfate groups at specific positions of its repeating unit, were obtained through multi-step, semi-synthetic strategies relying upon a sequence of regioselective protection, sulfation and deprotection steps. The structures of the obtained sulfated polysaccharides were fully characterized by ATR-FT-IR spectroscopy, CHNS elemental analysis, HP-SEC-MALLS and 2D-NMR spectroscopy. The structural analyses confirmed the pursued intermediate values for the global DS in all the three cases, together with unprecedented sulfation patterns. The binding affinity for some growth factors, relevant for biomedical applications (TGF-β1, BMP-2, VEGF and FGF-2), was then measured for the starting polysaccharides and the three sulfated derivatives thereof. The resulting structure-affinity correlation revealed – as expected – that the insertion of sulfate

groups within diabolican backbone is generally able to increase the binding strength. Noteworthy, within this frame some sulfation sites seemed to be much more effective than others to trigger the protein-polysaccharide interaction, at least with the FGF-2 growth factor. This result suggests a noteworthy, innovative conclusion, *i.e.* sulfation pattern could be a key structural element for the selective interaction with signaling proteins not only in the case of native GAGs, as already known, but also for GAG-like structures obtained by regioselective sulfation of naturally unsulfated polysaccharides. Further efforts are currently underway in our laboratories to prove this concept and find applications in the biomedical field, by enlarging the scope of regiochemically sulfated derivatives of natural polysaccharides from sustainable sources.

5. ACKNOWLEDGMENTS

This work was supported by Italian Ministry for University and Research (MUR) [grant number PRIN2022-PNR_P20224T45H]. SPR experiments were carried out using the facilities of the Montpellier Proteomics Platform (PPIM-PP2I, BioCampus Montpellier).

6. SUPPLEMENTARY MATERIAL

Copies of ^{1}H- and 2D-NMR spectra of the obtained derivatives.

7. REFERENCES

[1] D. Soares da Costa, R.L. Reis, I. Pashkuleva, Sulfation of glycosaminoglycans and its implications in human health and sisorders, Annu. Rev. Biomed. Eng. 19 (2017) 1–26. https://doi.org/10.1146/annurev-bioeng-071516-044610.

[2] C.L.R. Merry, U. Lindahl, J. Couchman, J.D. Esko, J. D., Proteoglycans and Sulfated Glycosaminoglycans, in: A.K. Varki, R.D. Cummings, J.D. Esko, P. Stanley, G.W. Hart, M.

Aebi, D. Mohnen, T. Kinoshita, N.H. Packer, J.H. Prestegard, R.L. Schnaar, P.H. Seeberger (Eds.), Essential of Glycobiology, fourth ed., Cold Spring Harbor Laboratory Press, Cold Spring Harbor, 2022, chapter 17.

[3] A. Köwitsch, G. Zhou, T. Groth, Medical application of glycosaminoglycans: A review, J. Tissue Eng. Regen. Med. 12 (2018) e23–e41. https://doi.org/10.1002/term.2398.

[4] O.F. Restaino, R. Finamore, A. Stellavato, P. Diana, E. Bedini, M. Trifuoggi, M. De Rosa, C. Schiraldi, 2019. European chondroitin sulfate and glucosamine food supplements: A systematic quality and quantity assessment compared to pharmaceuticals. Carbohydr. Polym. 222, 114984. https://doi.org/10.1016/j.carbpol.2019.114984.

[5] T.K. Kishimoto, K. Viswanathan, T. Ganguly, S. Elankumaran, S. Smith, K. Pelzer, K., J.C. Lansing, N. Sriranganathan, G. Zhao, Z. Galcheva-Gargova, A. Al-Hakim, G.S. Bailey, B. Fraser, S. Roy, T. Rogers-Cotrone, L. Buhse, M. Vhary, J. Fox, M. Nasr, G.J. Dal Pan, Z. Shriver, R.S. Langer, G. Venkataraman, K.F. Austen, J. Woodcock, R. Sasisekharan, Contaminated heparin associated with adverse clinical events and activation of the contact system, New. Engl. J. Med. 358 (2008) 2457–2467. https://doi.org/10.1056/NEJMoa0803200.

[6] Q. Ren, J. Wang, C. Liu, L. Meng, R. Qian, H. Gao, W. Qin, C. Zhou, S. Qiao, H. Wang, L. Zhang, Y. Zhang, 2021. Exploring the sulfate patterns of chondroitin sulfate/dermatan sulfate and keratan sulfate in human pancreatic cancer. J. Pharm. Biomed. Anal. 205, 114339. https://doi.org/10.1016/j.jpba.2021.114339.

[7] X. Han, P. Sanderson, S. Nesheiwat, L. Lin, Y. Yu, F. Zhang, I.J. Amster, R.J. Linhardt, Structural analysis of urinary glycosaminoglycans from healthy human subjects, Glycobiology 30 (2020) 143–151. https://doi.org/10.1093/glycob/cwz088.

[8] A. Badri, A. Williams, R.J. Linhardt, M.A.G. Koffas, The road to animal-free glycosaminoglycan production: current efforts and bottlenecks, Curr. Opin. Biotechnol. 53 (2018) 85–92. https://doi.org/10.1016/j.copbio.2017.12.018.

[9] W. Zhang, R. Xu, J. Chen, H. Xiong, Y. Wang, B. Pang, G. Du, Z. Kang, 2023. Advances and challenges in biotechnological production of chondroitin sulfate and its oligosaccharides. Int. J. Biol. Macromol. 253, 126551. https://doi.org/10.1016/j.ijbiomac.2023.126551.

[10] V.H. Pomin, A dilemma in the glycosaminoglycan-based therapy: Synthetic or naturally unique molecules?, Med. Res. Rev. 35 (2015) 1195–1216. https://doi.org/10.1002/med.21356.

[11] S. Perez, O. Makshakova, J. Angulo, E. Bedini, A. Bisio, J.L. de Paz Carrera, E. Fadda, M. Guerrini, M. Hricovini, M. Hricovini, F. Lisacek, P. Nieto, K. Pagel, G. Paiardi, R. Richter, S. Samsonov, R. Vives, D. Nikitovic, S. Ricard Blum, Glycosaminoglycans: what remains to be deciphered?, J. Am. Chem. Soc. Au 3 (2023) 628–656. https://doi.org/10.1021/jacsau.2c00569.

[12] J. Gottschalk, L. Elling, Current state on the enzymatic synthesis of glycosaminoglycans, Curr. Opin. Chem. Biol. 61 (2021) 71–80. https://doi.org/10.1016/j.cbpa.2020.09.008.

[13] X. Zhang, L. Lin, H. Huang, R.J. Linhardt, Chemoenzymatic synthesis of glycosaminoglycans, Acc. Chem. Res. 53 (2020) 335−346. https://doi.org/10.1021/acs.accounts.9b00420.

[14] X. Jin, W. Zhang, Y. Wang, J. Sheng, R. Xu, J. Li, G. Du, Z. Kang, Biosynthesis of non-animal chondroitin sulfate from methanol using genetically engineered *Pichia pastoris*, *Green Chem.* 23 (2021) 4365–4374. https://doi.org/10.1039/d1gc00260k.

[15] A. Badri, A. Williams, A. Awofiranye, P. Datta, K. Xia, W. He, K. Fraser, J.S. Dordick, R.J. Linhardt, M.A.G. Koffas, 2021. Complete biosynthesis of a sulfated chondroitin in *Escherichia coli*. Nat. Commun. 12, 1389. https://doi.org/10.1038/s41467-021-21692-5.

[16] D. Wang, L. Hu, R. Xu, W. Zhang, H. Xiong, Y. Wang, G. Du, Z. Kang, 2023. Production of different molecular weight glycosaminoglycans with microbial cell factories, Enzyme Microb. Technol. 171, 110324. https://doi.org/10.1016/j.enzmictec.2023.110324.

[17] E. Bedini, C. De Castro, M. De Rosa, A. Di Nola, A. Iadonisi, O.F. Restaino, C. Schiraldi, M. Parrilli, A microbiological-chemical strategy to produce chondroitin sulfate A,C, Angew. Chem. Int. Ed. 50 (2011) 6160–6163. https://doi.org/10.1002/anie.201101142.

[18] G. Vessella, S. Traboni, A. Laezza, A. Iadonisi, E. Bedini, 2020. (Semi)-Synthetic fucosylated chondroitin sulfate oligo- and polysaccharides. Mar. Drugs 18, 293. https://doi.org/10.3390/md18060293.

[19] D.K. Afosah, R.A. Al-Rohani, Sulfated non-saccharide glycosaminoglycan mimetics as novel drug discovery platform for various pathologies, Curr. Med. Chem. 27 (2020) 3412–3447. https//doi.org/10.2174/0929867325666181120101147.

[20] Q. Liu, G. Chen, H. Chen, Chemical synthesis of glycosaminoglycan-mimetic polymers, Polym. Chem. 10 (2019) 164–171. https://doi.org/10.1039/C8PY01338A.

[21] Ø. Arlov, D. Rütsche, M.A. Korayem, F. Öztürk, M. Zenobi-Wong, 2021. Engineered sulfated polysaccharides for biomedical applications. Adv. Funct. Mater. 2010732. https://doi.org/10.1002/adfm.202010732.

[22] K. Zeng, T. Groth, K. Zhang, Recent advances in artificially sulfated polysaccharides for applications in cell growth and differentiation, drug delivery, and tissue engineering, ChemBioChem 20 (2019) 737–746. https://doi.org/10.1002/cbic.201800569.

[23] M. Guerrini, D. Beccati, Z. Shriver, A. Naggi, K. Viswanathan, A. Bisio, I. Capila, J.C. Lansing, S. Guglieri, B. Fraser, A. Al-Hakim, N.S. Gunay, Z. Zhang, L. Robinson, L. Buhse, M. Nasr, J. Woodcock, R. Langer, G. Venkataraman, R.J. Linhardt, B. Casu, G. Torri, R. Sasisekharan, Oversulfated chondroitin sulfate is a contaminant in heparin associated with adverse clinical events, Nat. Biotechnol. 26 (2008) 669–675. https://doi.org/10.1038/nbt1407.

[24] E. Bedini, A. Laezza, M. Parrilli, A. Iadonisi, A review of chemical methods for the selective sulfation and desulfation of polysaccharides, Carbohydr. Polym. 174 (2017) 1224–1239. https://doi.org/10.1016/j.carbpol.2017.07.017.

[25] C. Delbarre-Ladrat, C. Sinquin, L. Lebellenger, A. Zykwinska, S. Colliec-Jouault, 2014. Exopolysaccharides produced by marine bacteria and their applications as glycosaminoglycan-like molecules. Front. Chem. 2, 85. https://doi.org/10.3389/fchem.2014.00085.

[26] K. Liu, L. Guo, X. Chen, L. Liu, C. Gao, Microbial synthesis of glycosaminoglycans and their oligosaccharides, Trends Microbiol. 31 (2023) 369–383. https://doi.org/10.1016/j.tim.2022.11.003.

[27] D. Cimini, E. Bedini, C. Schiraldi, 2023. Biotechnological advances in the synthesis of modified chondroitin towards novel biomedical applications. Biotechnol. Adv. 67, 108185. https://doi.org/0.1016/j.biotechadv.2023.108185.

[28] G. Raguénès, R. Christen, J. Guezennec, P. Pignet, G. Barbier, *Vibrio diabolicus* sp. Nov., a new polysaccharide-secreting organism isolated from a deep-sea hydrothermal vent polychaete annelid, *Alvinella pompejana*. Int. J. Syst. Evol. Microbiol. 47 (1997) 989–995. https://doi.org/10.1099/00207713-47-4-989.

[29] F. Benhadda, A. Zykwinska, S. Colliec-Jouault, C. Sinquin, B. Thollas, A. Courtois, N. Fuzzati, A. Toribio, C. Delbarre-Ladrat, 2023. Marine versus non-marine bacterial exopolysaccharides and their skincare applications. Mar. Drugs 21, 582. https://doi.org/10.3390/md21110582.

[30] F. Esposito, G. Vessella, C. Sinquin, S. Traboni, A. Iadonisi, S. Colliec-Jouault, A. Zykwinska, E. Bedini, 2022. Glycosaminoglycan-like sulfated polysaccharides from *Vibrio diabolicus* bacterium: semi-synthesis and characterization. Carbohydr. Polym. 283, 119054. https://doi.org/10.1016/j.carbpol.2021.119054.

[31] N. Veraldi, I. Dentand Quadri, Y. van de Looij, L. Malaguti Modernell, C. Sinquin, A. Zykwinska, B.B. Tournier, F. Dalonneau, H. Li, J.-P. Li, P. Millet, R. Vives, S. Colliec-Jouault, A. de Agostini, E. Farias Sanches, S.V. Sizonenko, 2023. Low-molecular weight sulfated marine polysaccharides: promising molecules to prevent neurodegeneration in

mucopolysaccharidosis IIIA?. Carbohydr. Polym. 320, 121214. https://doi.org/10.1016/j.carbpol.2023.121214.

[32] C. Delbarre-Ladrat, C. Sinquin, L. Marchand, S. Bonnetot, A. Zykwinska, V. Verrez-Bagnis, Sylvia Colliec-Jouault, 2022. Influence of the carbon and nitrogen sources on diabolican production by the marine *Vibrio diabolicus* Strain CNCM I-1629. Polymers 14, 1994. https://doi.org/10.3390/polym14101994.

[33] H. Rougeaux, N. Kervarec, R. Pichon, J. Guezennec, Structure of the exopolysaccharide of *Vibrio diabolicus* isolated from a deep-sea hydrothermal vent, Carbohydrate Res. 322 (1999) 40–45. https://doi.org/10.1016/s0008-6215(99)00214-1.

[34] K. Senni, F. Gueniche, S. Changotade, D. Septier, C. Sinquin, J. Ratiskol, D. Lutomski, G. Godeau, J. Guezennec, S. Colliec-Jouault, Unusual glycosaminoglycans from a deep sea hydrothermal bacterium improve fibrillar collagen structuring and fibroblast activities in engineered connective tissues. Mar. Drugs 11 (2013) 1351–1369. https://doi.org/10.3390/md11041351.

[35] A. Koschella, D. Klemm, Silylation of cellulose regiocontrolled by bulky reagents and dispersity in the reaction media, Macromol. Symp. 120 (1997) 115−125. https://doi.org/10.1002/masy.19971200113.

[36] F. Esposito, A. Laeuza, V. Gargiulo, S. Traboni, A. Iadonisi, A. La Gatta, C. Schiraldi, E. Bedini, Multi-step strategies toward regioselectively sulfated M-rich alginates, Biomacromolecules 24 (2023) 2522–2531. https://doi.org/10.1021/acs.biomac.3c00045.

[37] M. Schuler, A. Tatibouët, Strategies toward protection of 1,2- and 1,3-diols in carbohydrate chemistry, in: S. Vidal (Ed.) Protecting Group: Strategies and Applications in Carbohydrate Chemistry, John Wiley & Sons, Hoboken, 2018, pp. 307−335.

[38] G. Vessella, F. Esposito, S. Traboni, C. Di Meo, A. Iadonisi, C. Schiraldi, E. Bedini, 2021. Exploiting diol reactivity for the access to unprecedented low molecular weight sulfated curdlan

polysaccharides. Carbohydr. Polym. 269, 118324. https://doi.org/10.1016/j.carbpol.2021.118324.

[39] G. Vessella, S. Traboni, D. Cimini, A. Iadonisi, C. Schiraldi, E. Bedini, Development of semisynthetic, regioselective pathways for accessing the missing sulfation patterns of chondroitin sulfate, Biomacromolecules 20 (2019) 3021−3030. https://doi.org/10.1021/acs.biomac.9b00590.

[40] I. Speciale, A. Notaro, P. Garcia-Vello, F. Di Lorenzo, S. Armiento, A. Molinaro, R. Marchetti, A. Silipo, C. De Castro, 2022. Liquid-state NMR spectroscopy for complex carbohydrate structural analysis: a hitchhiker's guide. Carbohydr. Polym. 277, 118885. https://doi.org/10.1016/j.carbpol.2021.118885.

[41] V. Gargiulo, R. Lanzetta, M. Parrilli, C. De Castro, Structural analysis of chondroitin sulfate from *Scyliorhinus canicula*: a useful source of this polysaccharide, Glycobiology 19 (2009) 1485−1491. https://doi.org/10.1093/glycob/cwp123.

[42] M. Guerrini, A. Naggi, S. Guglieri, R. Santarsiero, G. Torri, Complex glycosaminoglycans: profiling substitution patterns by two dimensional nuclear magnetic resonance spectroscopy, Anal. Biochem. 337 (2005) 35−47. https://doi.org/10.1016/j.ab.2004.10.012.

[43] E.M. Bachelder, E.N. Pino, K.M. Ainslie, Acetalated dextran: a tunable and acid-labile biopolymer with facile synthesis and a range of applications, Chem. Rev. 117 (2017) 1915−1926. https://doi.org/10.1021/acs.chemrev.6b00532.

[44] A. Laezza, C. De Castro, M. Parrilli, E. Bedini, Inter *vs.* intraglycosidic acetal linkages control sulfation pattern in semi-synthetic chondroitin sulfate, Carbohydr. Polym. 112 (2014) 546−555. https://doi.org/10.1016/j.carbpol.2014.05.085.

[45] N.S. Gandhi, R.L. Mancera, The structure of glycosaminoglycans and their interactions with proteins, Chem. Biol. Drug Des. 72 (2008) 455−482. https://doi.org/10.1111/j.1747-0285.2008.00741.x.

[46] S.D. Vallet, C. Berthollier, S. Ricard-Blum, The glycosaminoglycan interactome 2.0, Am. J. Physiol. Cell Physiol. 322 (2022) 1271−1278. https://doi.org/10.1152/ajpcell.00095.2022.

[47] O.A. Ibrahimi, F.M. Zhang, S.C.L. Hrstka, M. Mohammadi, R.J. Linhardt, Kinetic model for FGF, FGFR, and proteoglycan signal transduction complex assembly, Biochemistry 43 (2004) 4724−4730. https://doi.org/10.1021/bi0352320.

[48] R. Raman, G. Venkataraman, S. Ernst, V. Sasisekharan, R. Sasisekharan, Structural specificity of heparin binding in the fibroblast growth factor family of proteins, Proc. Natl. Acad. Sci. U.S.A. 4 (2003) 2357–2362. https://doi.org/10.1073/pnas.0437842100.

[49] S. Guglieri, M. Hricovini, R. Raman, L. Polito, G. Torri, B. Casu, R. Sasisekharan, M. Guerrini, Minimum FGF2 binding structural requirements of heparin and heparan sulfate oligosaccharides as determined by NMR spectroscopy, Biochemistry 47 (2008) 13862–13869. https://doi.org/10.1021/bi801007p.

[50] J. Kreuger, M. Salmivirta, L. Sturiale, G. Gimenez-Gallego, U. Lindahl, Sequence analysis of heparan sulfate epitopes with graded affinities for fibroblast growth factors 1 and 2, J. Biol. Chem. 276 (2001) 30744–30752. https://doi.org/10.1074/jbc.M102628200.

[51] M. Rusnati, D. Coltrini, F. Caccia, P. Dell'Era, G. Zoppetti, P. Oreste, Distinct role of 2-*O*-, *N*-, and 6-*O*-sulfategroups of heparin in the formation of the ternary complex with basic fibroblast growth factor and soluble FGF receptor-1, Biochem. Biophys. Res. Commun. 203 (1994) 450–458. https://doi.org/10.1006/bbrc.1994.2203.

Table 1: Global yield and structural features of derivatives **SD-5-7**

	Semi-synthetic precursor	Yield[a]	M_w [kDa]	$Đ$[b]	DS[c]	Sulfation pattern[d]
LMW diabolican	--	--	24.0 ± 0.1	1.36 ± 0.02	0	--
SD-5	**6**	132%	15.8 ± 0.6	1.58 ± 0.11	3.85 ± 0.25 / 5.31	GalNAc-*O*-3 (1; 1) GalNAc-*O*-6 (1; 1) GlcA-*O*-2 (2; 1.31) GlcA-*O*-3 (2; 2)
SD-6	**8**	72%	6.7 ± 0.6	1.39 ± 0.17	2.80 ± 0.03 / 2.18	GlcA-*O*-3 (0; 0.19) GlcA-*O*-2 (0; 0.51) GlcNAc-*O*-4 (1; 0.48) GlcNAc-*O*-6 (1; 1)
SD-7	**10**	41%	11.5 ± 1.2	1.78 ± 0.28	1.27 ± 0.16 / 0.62	GalNAc-*O*-3 (0; 0.20) GlcA-*O*-3 (2; 0) GlcNAc-*O*-4 (0; 0.42)

[a] Overall weight yield calculated from starting LMW diabolican.

[b] Calculated as the ratio between M_w and M_n.

[c] Degree of sulfation (as average percentage amount of sulfate groups per diabolican repeating unit) evaluated by CHNS elemental analysis (first value) or estimated by 2D-NMR analysis (second value).

[d] Values in parenthesis refer to DS per single site (average percentage amount of sulfate groups installed per single position of the repeating unit) as expected theoretically (first value; see also Fig. 3) or estimated by 2D-NMR analysis (second value; see text for details). If both experimental and theoretical values were zero, the related positions were omitted.

Table 2: ^{1}H and ^{13}C NMR chemical shift[a,b] attribution of semi-synthetic derivatives **SD-5-7** and comparison with LMW unsulfated and per-*O*-sulfated diabolican polysaccharides [30]

	Subunit	**1**	**2**	**3**	**4**	**5**	**6**	***Other signals***
SD-5	*GalNAc3,6S*	5.56 *97.8*	4.45/4.57[c] *49.4*	4.47 *75.8*	4.47 *74.7*	4.07 *70.3*	4.15/4.22 *69.8*	NAc 1.97–2.03/ *23.3-23.7*
	→4)-GlcA2,3S-(1→4)-GalNAc3,6S	5.07 *101.4*	4.34 *78.5*	4.71 *78.9*	4.24 *78.7*	n.d.[d]	---	
	→4)-GlcA3S-(1→4)-GalNAc3,6S	4.80 *103.5*	3.60 *73.3*	4.48 *82.8*	4.11 *74.7*	n.d.[d]	---	
	GlcNAc-(1→4)-GlcA2,3S	4.91/4.95[c] *101.6*	4.34/4.38[c] *78.5*	4.93 *77.6*	4.42 *78.3*	n.d.[d]	---	
	GlcNAc	4.66 *103.0*	3.82 *55.5*	3.75 *79.1*	3.67 *72.3*	3.38 *77.2*	3.68/3.84 *61.8*	
SD-6	*GalNAc*	5.24/5.43[c] *98.7/99.1[c]*	4.25 *51.6*	3.91 *68.9*	4.22 *77.6*	n.d.[d]	3.66/3.80 *61.1*	NAc 2.03– 2.08/*23.6*
	→4)-GlcA-(1→4)-GalNAc	4.68 *104.4*	3.47 *74.2*	3.68 *75.4*	3.74 *82.0*	3.83 *76.4*	---	
	→4)-GlcA3S-(1→4)-GalNAc	4.76 *104.2*	3.68 *73.9*	4.43 *82.5*	4.06 *77.4*	n.d.[d]	---	
	GlcNAc4,6S-(1→4)-GlcA	4.53 *103.5*	3.31 *73.9*	3.60 *75.1*	3.75 *77.3*	n.d.[d]	---	
	GlcNAc4,6S-(1→4)-GlcA2S	4.60 *103.2*	4.33 *84.6*	3.69 *n.d.[d]*	n.d.[d]	n.d.[d]	---	
	GlcNAc4,6S	4.60 *102.6*	3.78 *55.0*	n.d.[d]	4.44 *78.1*	3.93 *73.5*	4.19/4.56 *68.4*	
	GlcNAc6S	4.57 *101.6*	3.83 *55.8*	n.d.[d]	n.d.[d]	n.d.[d]	4.27/4.35 *67.9*	
SD-7	*GalNAc*	5.19/5.41[c] *98.5/99.5[c]*	4.27 *51.6*	3.89 *68.9*	4.23 *77.7*	3.84 *71.7*	3.67/3.83 *61.2*	NAc 2.04– 2.07/*23.7*
	GalNAc3S	5.42 *98.5*	4.48 *49,6*	4.53 *76.3*	4.51 *74.0*	n.d.[d]	3.81/3.89 *61.6*	
	→4)-GlcA-(1→4)-GalNAc	4.69/4.75[c] *103.8/104.5[c]*	3.47 *74.4*	3.60 *75.3*	3.72 *82.0*	n.d.[d]	---	
	GlcNAc-(1→4)-GlcA	4.55 *103.9*	3.37 *74.1*	3.60 *75.3*	3.80 *81.2*	n.d.[d]	---	
	GlcNAc	4.59 *101.6*	3.78 *55.4*	3.71 *79.6*	3.72 *72.2*	3.46 *77.0*	3.74/3.91 *61.7*	
	GlcNAc4S	4.59 *101.6*	3.87 *56.2*	4.00 *78.4*	4.42 *78.1*	3.59 *73.6*	3.83/3.99 *61.8*	
LMW diabolican	*GalNAc*	5.42 *99.0*	4.27 *51.3*	3.89 *69.2*	4.22 *77.6*	3.83 *71.9*	3.66/3.83 *61.3*	NAc 2.00– 2.06/*23.4*
	→4)-GlcA-(1→4)-GalNAc	4.68 *104.7*	3.46 *74.6*	3.60 *75.3*	3.67 *82.6*	3.84 *76.6*	---	
	GlcNAc-(1→4)-GlcA	4.53 *104.2*	3.36 *74.5*	3.60 *75.3*	3.75 *80.7*	3.75 *77.9*	---	
	GlcNAc	4.58 *101.8*	3.77 *55.4*	3.67 *79.4*	3.65 *72.5*	3.45 *77.5*	3.73/3.92 *61.8*	
LMW per-*O*-sulfated diabolican[a]	*GalNAc3,6S*	5.60 *97.5*	4.68 *48.5*	4.44 *76.6*	4.57 *73.7*	4.16 *70.1*	4.22/4.29 *69.5*	NAc 2.02/*23.6* 2.10/*23.7*
	→4)-GlcA2,3S-(1→4)-GalNAc3,6S	5.15 *n.d.[d]*	4.42 *n.d.[d]*	4.81 *78.6*	4.34 *78.5*	n.d.[d]	---	
	GlcNAc4,6S-(1→4)-GlcA2,3S	5.00 *102.3*	4.46 *n.d.[d]*	4.72 *78.1*	4.24 *78.2*	n.d.[d]	---	
	GlcNAc4,6S	4.80 *100.9*	4.01 *55.2*	4.11 *76.0*	4.49 *79.2*	3.92 *73.9*	4.21/4.63 *68.5*	

[a] NMR experiments conducted in D_2O (600 MHz, 298 K).

[b] Chemical shift values are expressed in δ relative to internal acetone (^{1}H: $(CH_3)_2CO$ at δ = 2.22 ppm; ^{13}C: $(CH_3)_2CO$ at δ = 31.5 ppm).

[c] These atoms show two signals at different ^{1}H and/or ^{13}C-chemical shifts presumably due to a different structure of a neighbouring residue.

[d] Not determined.

Table 3: Dissociation constant (Kd) values showing the binding affinity between diabolican derivatives and growth factors.

	***Kd (M)* TGF-β1**	***Kd (M)* BMP-2**	***Kd (M)* VEGF**	***Kd (M)* FGF-2**
LMW diabolican [30]	$9.1\ 10^{-8}$	$3.5\ 10^{-8}$	$1.7\ 10^{-8}$	$4.0\ 10^{-8}$
SD-4 [30]	$4.8\ 10^{-10}$	$6.2\ 10^{-10}$	$7.7\ 10^{-10}$	$2.6\ 10^{-9}$
SD-5	$3.4\ 10^{-9}$	$2.3\ 10^{-9}$	$2.9\ 10^{-8}$	$9.6\ 10^{-10}$
SD-6	$3.1\ 10^{-9}$	$5.8\ 10^{-9}$	$4.1\ 10^{-8}$	$>10^{-5}$
SD-7	$2.2\ 10^{-9}$	$4.2\ 10^{-9}$	$1.3\ 10^{-8}$	$4.6\ 10^{-8}$

LIST OF GRAPHICS CAPTIONS

Figure 1: Chemical structure of diabolican polysaccharide and its already obtained sulfated derivatives [30].

Figure 2: ^{1}H-NMR spectra of LMW diabolican (black) and semi-synthetic intermediates **6** (blue), **7** (red), **8** (green) and **9** (purple) (600 MHz, 298K, D_2O for LMW diabolican and **8** or DMSO-d_6 for **6**, **7** and **9**).

Figure 3: Chemical structure of target sulfated diabolican derivatives (green or grey signs indicate, respectively, the confirmation or not of sulfate groups at the expected positions; atom labels enclosed in dotted lines indicate the detected sulfate or hydroxyl group in disagreement with the expected structure; see Table 1 for detected DS values per single site).

Figure 4: Zoomed superimposition of A) ^{1}H-NMR, ^{1}H-^{13}C-DEPT-HSQC (black and red) and ^{1}H-^{13}C- HSQC-TOCSY (blue and green) and B) ^{1}H-NMR, COSY (black), TOCSY (red) and NOESY (green) 2D-NMR spectra (600 MHz, 298K, D_2O) of sulfated derivative **SD-5** (*GlcA$_I$* = GlcNAc-1→4-*GlcA2,3S*, *GlcA$_{II}$* = *GlcA2,3S*-1→4-GalNAc, *GlcA$_{III}$* = *GlcA3S*-1→4-GalNAc; densities enclosed in dotted lines were integrated for $GlcA_{II}$- $GlcA_{III}$ ratio estimation; only some assignments and correlations are indicated; see Table 2 for full chemical shift assignments).

Scheme 1: Multi-step approaches for the regioselective protection of LMW diabolican with bulky protecting groups (highlighted in blue).

Scheme 2: Multi-step approaches for the regioselective protection of LMW diabolican with cyclic protecting groups (highlighted in blue).

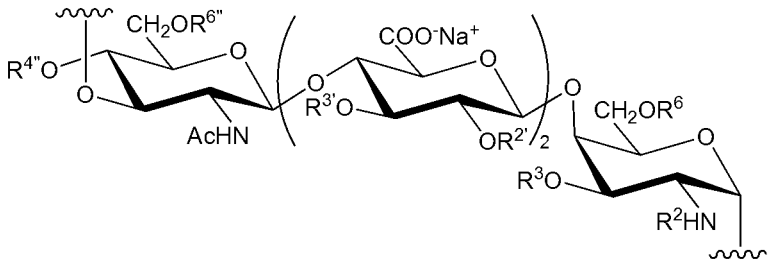

LMW diabolican: R^2 = Ac; $R^{2'}$, R^3, $R^{3'}$, $R^{4''}$, R^6, $R^{6''}$ = H; M_w = 24.0 kDa; DS = 0
SD-1: R^2 = Ac; $R^{2'}$, $R^{3'}$, $R^{4''}$ = H; R^3, R^6, $R^{6''}$ = H or $SO_3^-Na^+$; M_w = 27.2 kDa; DS = 1.5
SD-2: R^2 = $SO_3^-Na^+$; $R^{2'}$, R^3, $R^{3'}$, $R^{4''}$, R^6, $R^{6''}$ = H; M_w = 5.4 kDa; DS = 1
SD-3, SD-4: R^2 = Ac; $R^{2'}$, R^3, $R^{3'}$, $R^{4''}$, R^6, $R^{6''}$ = $SO_3^-Na^+$; M_w = 38.9 (**SD-3**), 12.3 kDa (**SD-4**); DS = 8

Figure 1

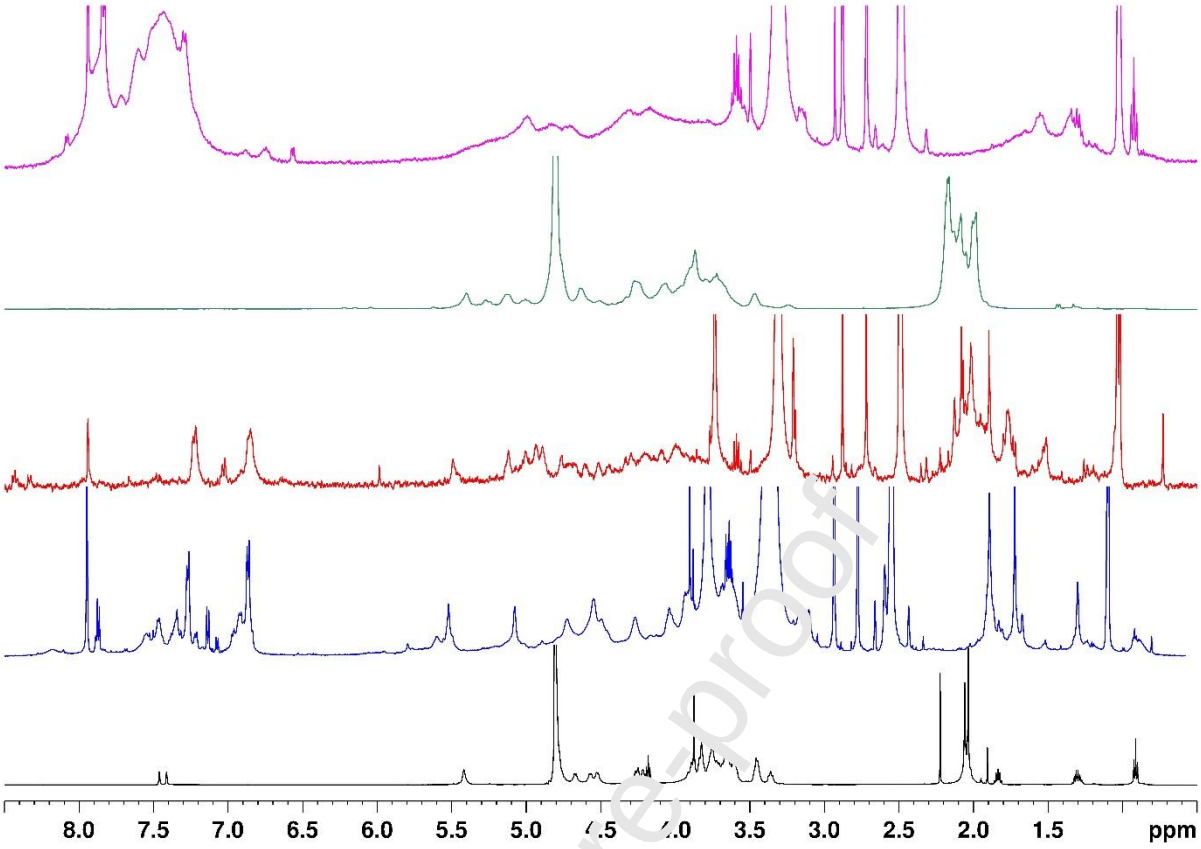

Figure 2

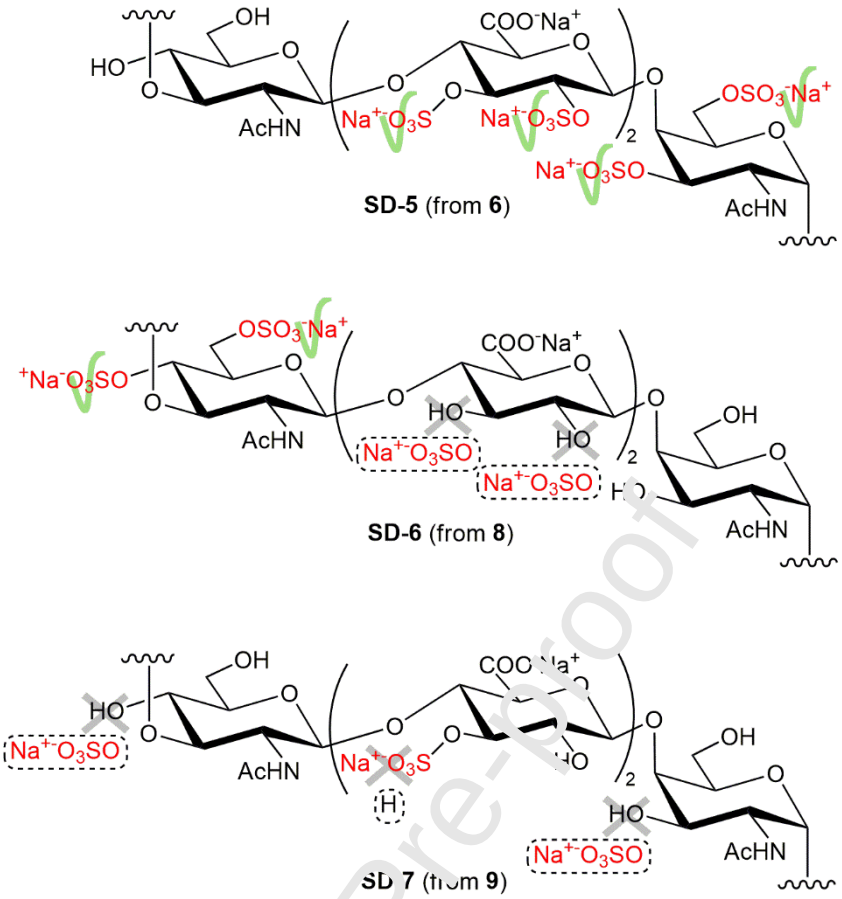

Figure 3

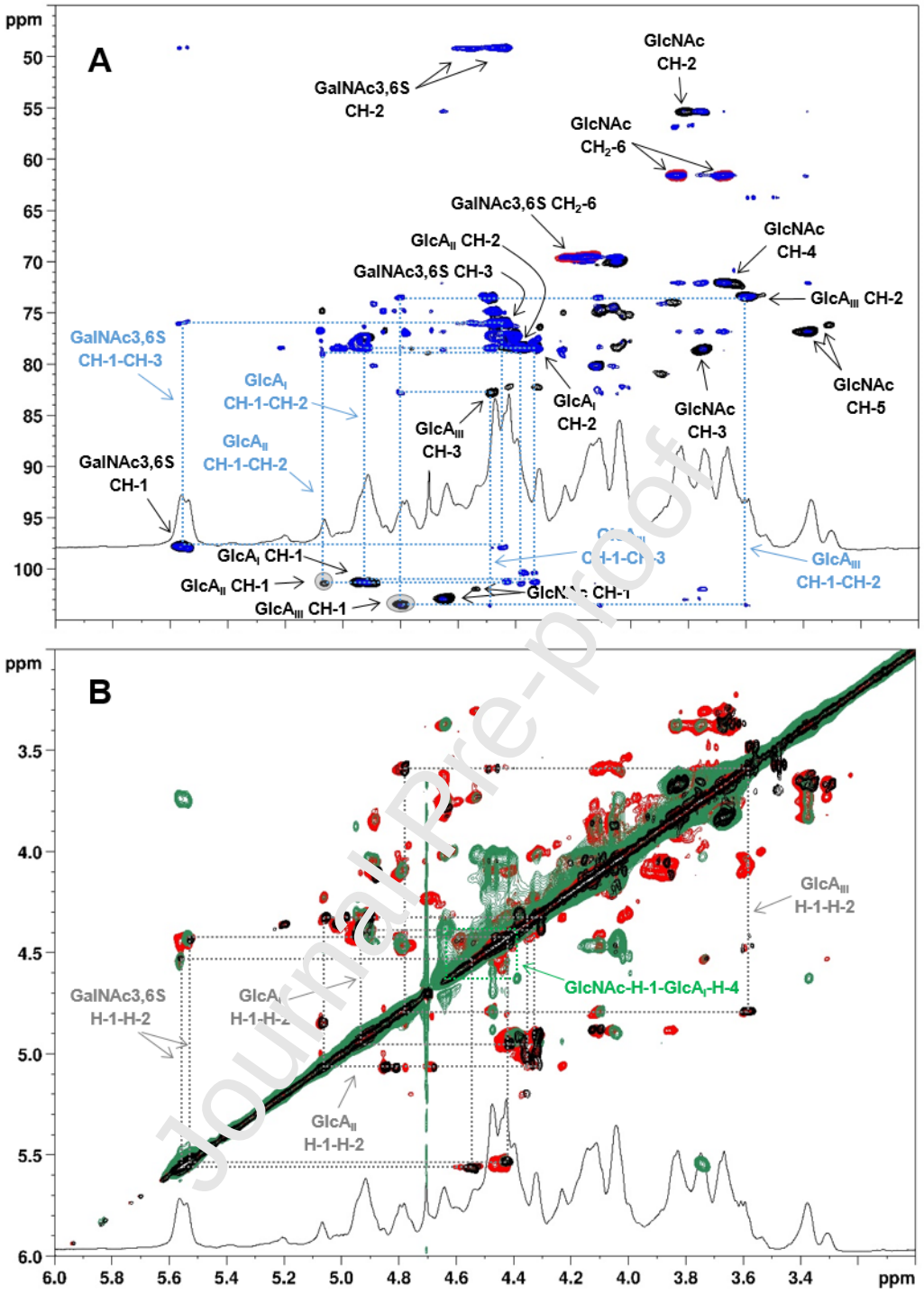
A
ppm
GalNAc3,6S CH-2
GlcNAc CH-2
GlcNAc CH2-6
GalNAc3,6S CH2-6
GlcAII CH-2
GalNAc3,6S CH-3
GlcNAc CH-4
GlcAIII CH-2
GalNAc3,6S CH-1-CH-3
GlcAI CH-1-CH-2
GlcAII CH-1-CH-2
GalNAc3,6S CH-1
GlcAIII CH-3
GlcAI CH-2
GlcNAc CH-3
GlcNAc CH-5
GlcAI CH-1
GlcAII CH-1
GlcAIII CH-1
GlcAIII CH-1-CH-2
B
ppm
GlcAIII H-1-H-2
GalNAc3,6S H-1-H-2
GlcNAc-H-1-GlcAI-H-4
GlcAII H-1-H-2
6.0 5.8 5.6 5.4 5.2 5.0 4.8 4.6 4.4 4.2 4.0 3.8 3.6 3.4 ppm

Figure 4

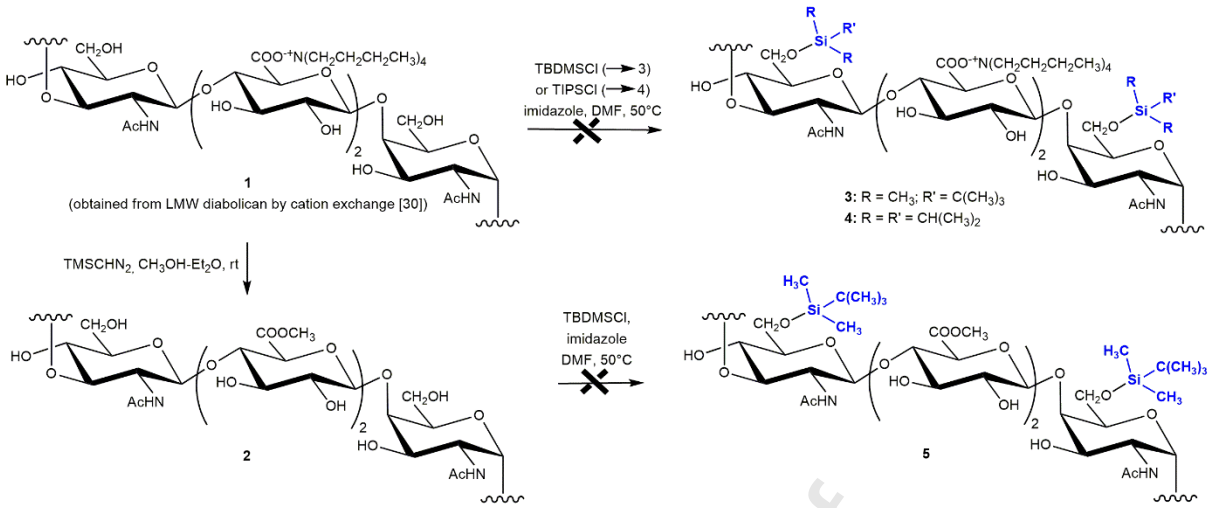

Scheme 1

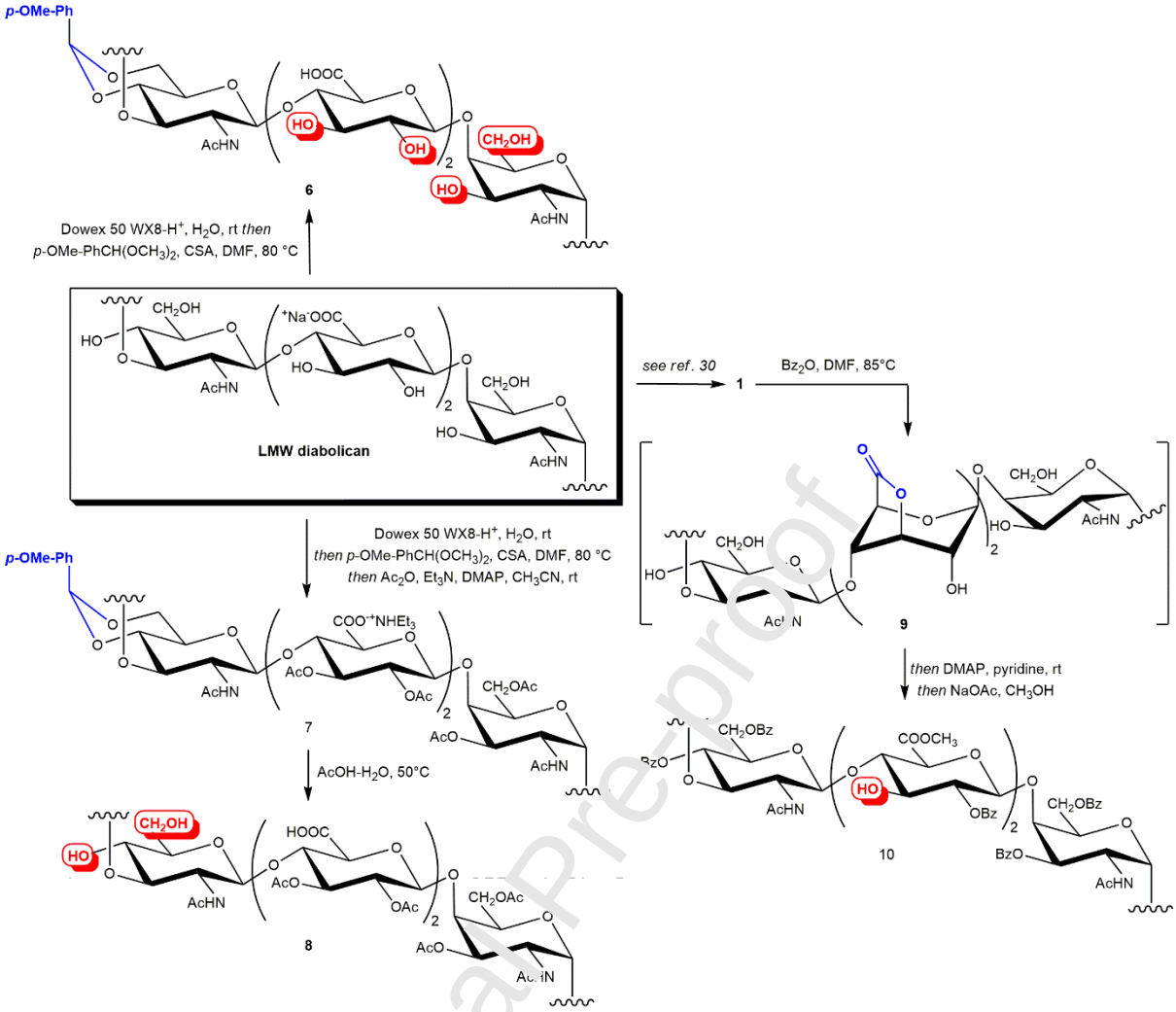

Scheme 2